Retina

Spatial Characteristics of Peripheral Visual Islands in Retinitis Pigmentosa

Tapan P. Patel,[1] Hursuong Vongsachang,[1] Andrew Schilling,[1] Xiangrong Kong,[1,2] and Mandeep S. Singh[1]

[1]Wilmer Eye Institute, Johns Hopkins University School of Medicine, Baltimore, Maryland, United States
[2]Johns Hopkins University Bloomberg School of Public Health, Baltimore, Maryland, United States

PURPOSE. Retinitis pigmentosa (RP) is typified by progressive peripheral visual field (pVF) loss in patterns that can vary between individuals. Greater understanding of pVF preservation may inform research on therapeutic targets. However, characteristics of retained pVF are incompletely understood. We aimed to evaluate the spatial characteristics of retained pVF in RP.

METHODS. We developed a computational platform to generate a probability map of the spatial distribution of retained pVF loci using the Goldmann V4e isopter. RP subjects were grouped into cross-sectional and longitudinal datasets. Probability maps of retained pVF were generated for categories of symptomatic disease duration (SDD). We applied a mathematical model to determine the anatomical correlate of the retained pVF.

RESULTS. A total of 152 subjects were included. The mean age was 46.7 years. SDD was <20 years (47.4%), 20 to 40 years (39.5%), or >40 years (13.2%). Longitudinal data (3.2–5.7 years of follow up) were available for 65 subjects. In the cross-sectional dataset, retained pVF loci were most likely to be located between the 50° and 80° isoeccentric meridians and between the 30° to 50° radial axes. In the longitudinal dataset, inferotemporal pVF loci were the most likely to be preserved over time. The area of pVF retention corresponded anatomically to the pre-equatorial superonasal retina.

CONCLUSIONS. Semiautomated quantitation of pVF may be a useful tool to analyze spatial characteristics of VF in RP. Retinal cells in the superonasal periphery may be resilient to RP-related functional decline. Understanding the cellular and molecular basis of pVF resilience in the retina may inform efforts to develop treatment modalities for RP.

Keywords: perimetry, retinal dystrophy, gene therapy, low vision, neuroprotection

Retinitis pigmentosa (RP) is a term that encompasses a heterogeneous group of inherited degenerative retinal diseases that are characterized by progressive visual field constriction.[1] Currently, there are no effective disease-modifying treatments available. Although many patients retain good central visual acuity during the natural history of RP, progressive mid-peripheral visual field (pVF) loss typically occurs.[2,3] Residual portions of the pVF, often referred to as peripheral islands of vision, indicate residual functional capacity of the peripheral retina. Recent data from the Center for Eye Research Australia indicated that many late-stage RP patients with poor visual acuity who were considered for inclusion in the Bionic Eye Study had peripheral islands of vision in one or both eyes.[4] Undetectable full-field electroretinography responses in most of those eyes indicated that widespread retinal degeneration had occurred, yet localized parts of the peripheral retina remained functionally resilient.

A rich body of work has provided information regarding quantitative and qualitative characteristics of VF loss in patients with RP. The canonical pattern of RP progression is such that retinal function degrades initially in the mid-peripheral VF and later involves the central portion.[3,5–8] However, variations of the canonical pattern have been described, including concentric VF loss, superior VF loss with nasal or temporal arcuate expansion, and complete or incomplete mid-peripheral ring scotoma with peripheral expansion.[5] Berson and colleagues studied 94 subjects with RP over 3 years and found that 4.6% of VF area was lost per year.[9] In a study by Grover et al.,[5] the pattern of VF loss influenced the rate of VF loss. In contrast, Fishman and colleagues[10] studied the VF loss in Usher syndrome type 2 and found that the pattern of VF loss did not affect the rate of VF loss. These studies and others underscored the importance of VF loss as a biomarker of disease severity and progression and indicated that the location of initial VF loss can vary among individuals with RP.

Variations in the angular and anteroposterior locations of VF loss initiation and progression suggest that parts of the peripheral retina may be differentially susceptible to RP-related damage. Greater understanding of localized peripheral retinal susceptibility/resilience in RP may yield insights into cellular and molecular mechanisms that promote localized retinal cell survival or function. These mechanisms may

inform future efforts to discover druggable molecular targets or to develop cell-based and gene-based treatment strategies to modify RP progression. However, gaps exist in the knowledge regarding the spatial features and clinical correlations of preserved pVF. To address these gaps and facilitate further research on peripheral retinal resilience in the retina, we asked the questions, "Probabilistically, where in the pVF do RP patients tend to retain function? Anatomically, which part or zone of the peripheral retina corresponds to the probabilistically retained pVF?"

To enable our research, we developed a semiautomated computational platform to quantify the spatial characteristics of pVF in RP using Goldmann visual field (GVF) plots extracted from electronic medical records. Specifically, we aimed to (1) determine the spatial localization of pVF regions that showed the maximal probability of preservation, (2) characterize the association of symptom duration with pVF preservation, and (3) estimate the anatomical location of the retinal region that correlated with pVF retention.

METHODS

Study Setting, Subjects, and Data Extraction

This retrospective observational study adhered to the tenets of the Declaration of Helsinki and was approved by the Johns Hopkins School of Medicine Institutional Review Board. Subjects with a clinical diagnosis of RP who were evaluated at the Wilmer Eye Institute between 2012 and 2020 and who had at least one GVF with a detectable Goldmann V4e isopter were included. The clinical diagnosis of RP was determined by an inherited retinal diseases specialist, based on a combination of all available clinical data including symptoms of nyctalopia or peripheral vision loss, mid-peripheral pigmentary retinopathy on biomicroscopy or imaging studies, visual field constriction, and scotopic full-field electroretinogram reduction that was greater than photopic reduction. GVFs, having been recorded according to the standard protocol,[7,11] were extracted as PDFs from the electronic case records. The cross-sectional dataset included the first (or only) GVF of that subject. If serial GVFs were available for a subject, the first and last available GVFs of that subject were included in the longitudinal dataset if the interval between them was at least 2 years. Where available, genetic testing results were recorded. In all cases, genetic testing was obtained from Clinical Laboratory Improvement Amendments–certified clinical diagnostic laboratories. For the purposes of this study, genetic test results were deemed confirmatory if mutations were classified as being pathogenic or likely pathogenic according to American College of Medical Genetics and Genomics guidelines[12] and were consistent with the RP phenotype. In cases of autosomal recessive alleles, homozygosity or compound heterozygosity was required and segregation analysis was not routinely performed.

Image Alignment

We developed a custom-coded algorithm in MATLAB (MathWorks, Natick, MA, USA) to quantify the spatial distribution of peripheral islands of vision. The GVFs of the right and left eyes were analyzed separately. Both eyes of each participant were included in the study, because potential differences in RP severity, lens status, media opacity, macular edema, and other comorbidity factors that were unique to each eye could have potentially contributed to VF findings. Scanned copies of the subjects' GVFs were aligned to a blank GVF grid centered on fixation using an affine transformation. The affine transformation used control points in the source and target image and a set of translation, rotation, and shear transformations to align both the source and target images to a common coordinate system. This resulted in a set of GVFs that were aligned such that pixel location in each scan corresponded to the same axis and eccentricity for all GVF images. The accuracy of image alignment was evaluated by manually selecting the pixel locations of three predefined points on the grid, located at (0,0), (40,0), and (0,40). Thirty randomly selected aligned GVFs were used for the right and left eyes. For each image, the distances in pixel values of the above predefined grid locations were recorded. The root mean square deviation of the set of pixel locations for each grid location was computed to determine the accuracy of image alignment.

Definition, Segmentation, and Probabilistic Mapping of Retained pVF

For the purposes of this study, retained pVF was defined as areas of remaining sensitivity to the V4e stimulus of standard kinetic Goldmann perimetry. The V4e isopter was manually traced for each GVF to generate a binary segmentation map of retained pVF (Fig. 1). The binary retained pVF segmentation map consisted of 0's (black) and 1's (white), which represented absent or present detection of the V4e stimulus, respectively. Because all of the GVFs were co-registered, the segmentation maps were averaged to generate a probability map of retained pVF (ranging from 0 to 1). For example, a value of 0.8 at point (x,y) on the aligned GVF grid indicated that 80% of subjects were able to detect the V4e stimulus at this location. To identify regions of high-probability pVF retention, we sampled the probability map along the radial and circumferential dimensions to generate two-dimensional plots of the probability of retained pVF as a function of stimulus location. For the circumferential dimension, nine separate curves were generated, corresponding to the 10°, 20°, 30°, …, 90° isoeccentric meridians. For each meridian, points were sampled at 1° intervals. Similarly, for the radial axis dimension, 36 curves were generated, corresponding to 10° intervals in the radial dimension around the circle. For each curve, 90 points were sampled along the line from the center of the grid to the 90° meridian.

The patterns of VF loss in our cohort were grouped as follows: (1) only a central island of remaining VF within 30° of fixation; (2) only peripheral island(s) of remaining VF, outside 30° of fixation; (3) both central and peripheral islands with complete or incomplete midperipheral scotomas; or (4) concentric constriction of VF outside 30° of fixation. For the purposes of this study, probability maps were generated from GVFs in groups 2 and 3 to specifically interrogate the locations of preserved pVF.

To address the heterogeneity of disease duration in this cohort, subjects were categorized by self-reported symptomatic disease duration (SDD). The year of self-reported onset of symptoms (typically, nyctalopia or pVF loss) for each subject was extracted from the chart. For the purposes of this study, we defined SDD as the time interval, in years, from symptom onset to the first GVF included in the dataset. SDD was categorized as <20 years, 20 to 40 years, and >40 years. The first-visit GVF image for each category of SDD was used for the cross-sectional analysis. Probability maps were generated for the subgroups of images defined by SDD category.
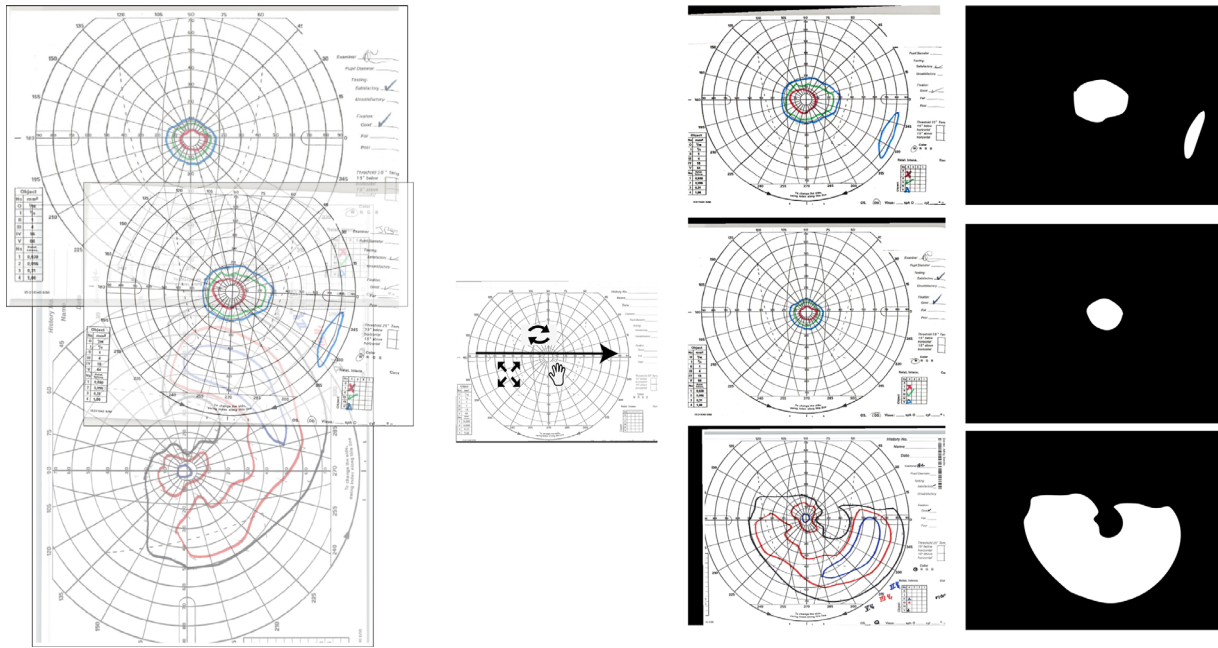
FIGURE 1. Computational process of GVF image alignment and segmentation. (*Left column*) Scanned copies of historical GVFs tended to vary in size and rotational alignment. (*Middle column*) GVFs were aligned to a blank template standard via a process involving rotation, translation, and shearing transformations. (*Right column*) The V4e isopter was manually traced for each GVF to a generate a binary segmentation map for each eye of each subject.

Longitudinal Analysis

A subset of subjects who had a second (follow-up) GVF at least 2 years apart from the first (baseline) GVF were included in the longitudinal analysis. The V4e isopter segmentation map of the second GVF was compared with the first GVF using the AND logic operator to identify loci of preserved pVF over time for each eye. Pixels that were present (1) at baseline and present (1) at follow-up were assigned "1" in the change map. Pixels that were present (1) at baseline but absent (0) at follow-up were assigned "0" in the change map. Subject-specific longitudinal change maps were averaged to produce a cohort longitudinal change map.

Statistics

Aggregate summaries of the data, including means, standard deviations, and medians, were generated with MATLAB. The Image Processing Toolbox of MATLAB was used for affine transformation, registration validation, and generation of probability maps.

RESULTS

A total of 152 right eyes and 149 left eyes of 152 subjects were included in this study. The mean age was 46.7 years, and 49.3% of the subjects were male. We did not detect a correlation between age and total area of the V4e isopter. Clinical and genotypic characteristics are summarized in the Table. The mean SDD at the first GVF visit was 22.7 ± 17.2 years. Disease-causing mutation(s) were found in the following genes: *ABCA4*, *BBS1*, *CDHR1*, *CRB1*, *EYS*, *FAM161A*, *NRL*, *PDE6B*, *PRPF31*, *PRPH2*, *RHO*, *RP1*, *RPGR*, *SAG*, and *USH2A*. For each causative mutation, the clinical and electrophysiological phenotype was confirmed as being compatible with RP.

TABLE. Subject Characteristics ($N = 152$)

Characteristic	
Age (y), mean (SD)	46.7 (17.5)
Sex (male), *n* (%)	75 (49.3)
Self-reported symptomatic disease duration (y), mean (SD)	22.7 (17.2)
Genotyping, *n* (%)	
Positive	68 (44.8)
Negative or inconclusive	21 (13.8)
No data available	63 (41.4)
Subjects with longitudinal data, *n* (%)	65 (42.8)

Each set of GVFs was co-registered to a blank GVF grid using iterative affine transformations (Fig. 1). The accuracy of image alignment, as assessed by the root mean square deviation of manual selection of predefined grid locations, was 4.3×5.1 pixels. For reference, the distance from grid location (0,0) to (10,0) was 44 pixels.

We generated two-dimensional probability maps of retained pVF by averaging the segmentation maps for the right and left eyes separately (Fig. 2). By analyzing the probability map of the right eyes across the radial and circumferential GVF dimensions, we identified a zone, located between the 50° and 80° isoeccentric meridians and between the 30° and 50° radial axes, that showed the highest probability of retained pVF (Figs. 2C–2F). This zone was located in the inferotemporal periphery of the visual field, and a laterally symmetrical zone was identified in the left eye (data not shown).

Patterns of VF were classified into one of four groups as described above. There were 46 right eyes (30%) and 49 left eyes (33%) with only central islands within 30° of fixation, six right eyes (4%) and two left eyes (1%) with only peripheral islands outside 30° of fixation, 40 right eyes (26%) and
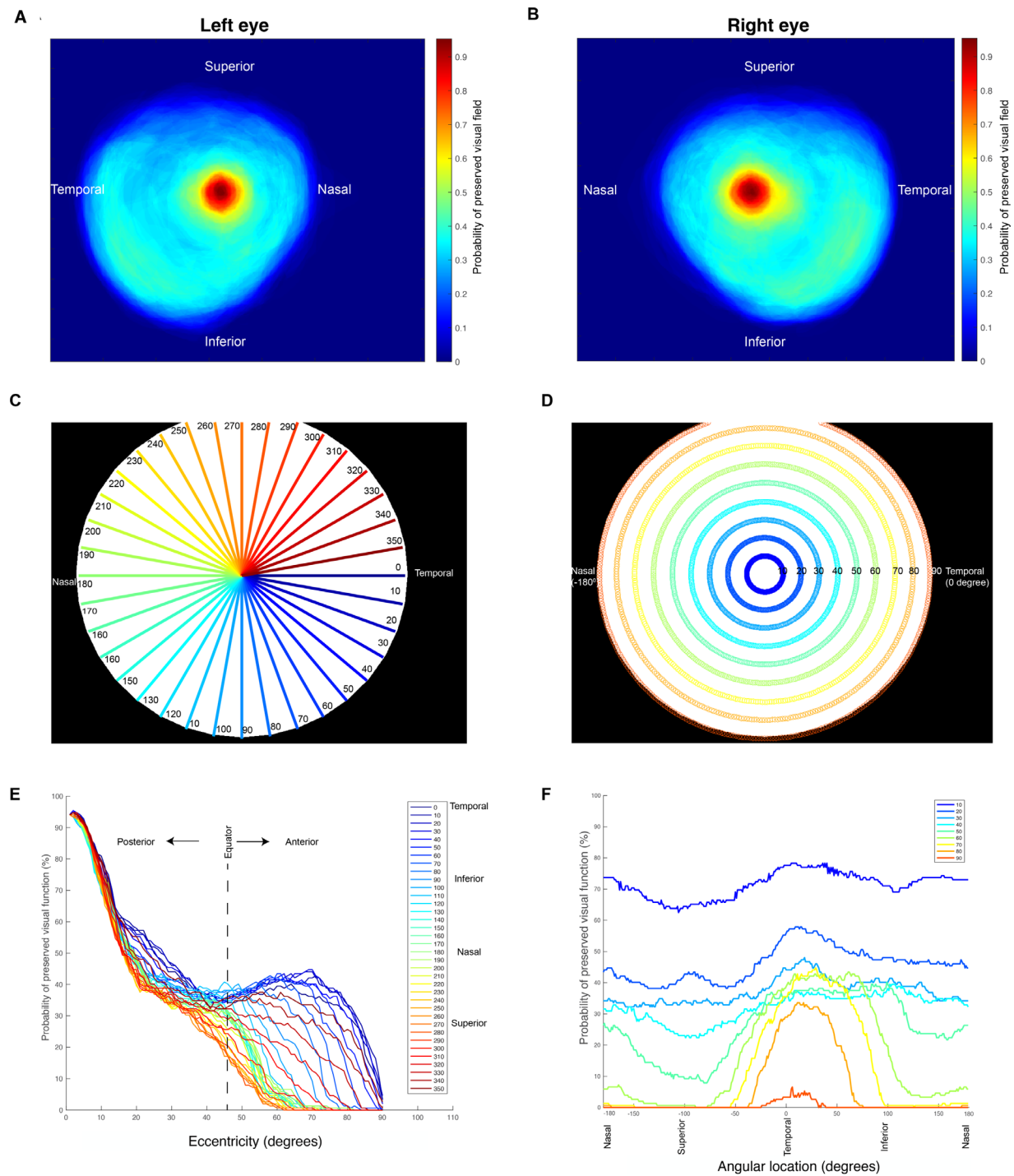
FIGURE 2. Spatial distribution of preserved pVF along radial and circumferential dimensions. The binary segmentation maps, based on the V4e isopter of all subjects, were averaged to generate a probability map of preserved VF areas for the left (**A**) and right (**B**) eyes. The probability of pVF preservation of the right eye was quantified along the radial (**C**) and circumferential (**D**) dimensions to identify the radial axes and isoeccentric meridians that defined the preserved pVF. (**E**) Probabilistic analysis along the radial axes showed that the highest probability of pVF preservation was within 10° of fixation and a lower peak of probability was located at approximately 70° eccentricity from fixation. (**F**) Probabilistic analysis along the isoeccentric meridians showed that the highest probability of pVF preservation occurred in the inferotemporal quadrant of the pVF.

42 left eyes (28%) with both central and peripheral islands with either complete or incomplete midperipheral scotomas, and 60 right eyes (39%) and 56 left eyes (38%) with concentric VF constriction outside 30° of fixation. Probability maps of pVF preservation of those with only peripheral islands

and those with both central and peripheral islands were similar between the right and left eyes (Fig. 3).

Sixty-eight subjects had a positive genetic test that confirmed the presence of disease mutation(s). For initial analysis, these subjects were categorized into two groups:
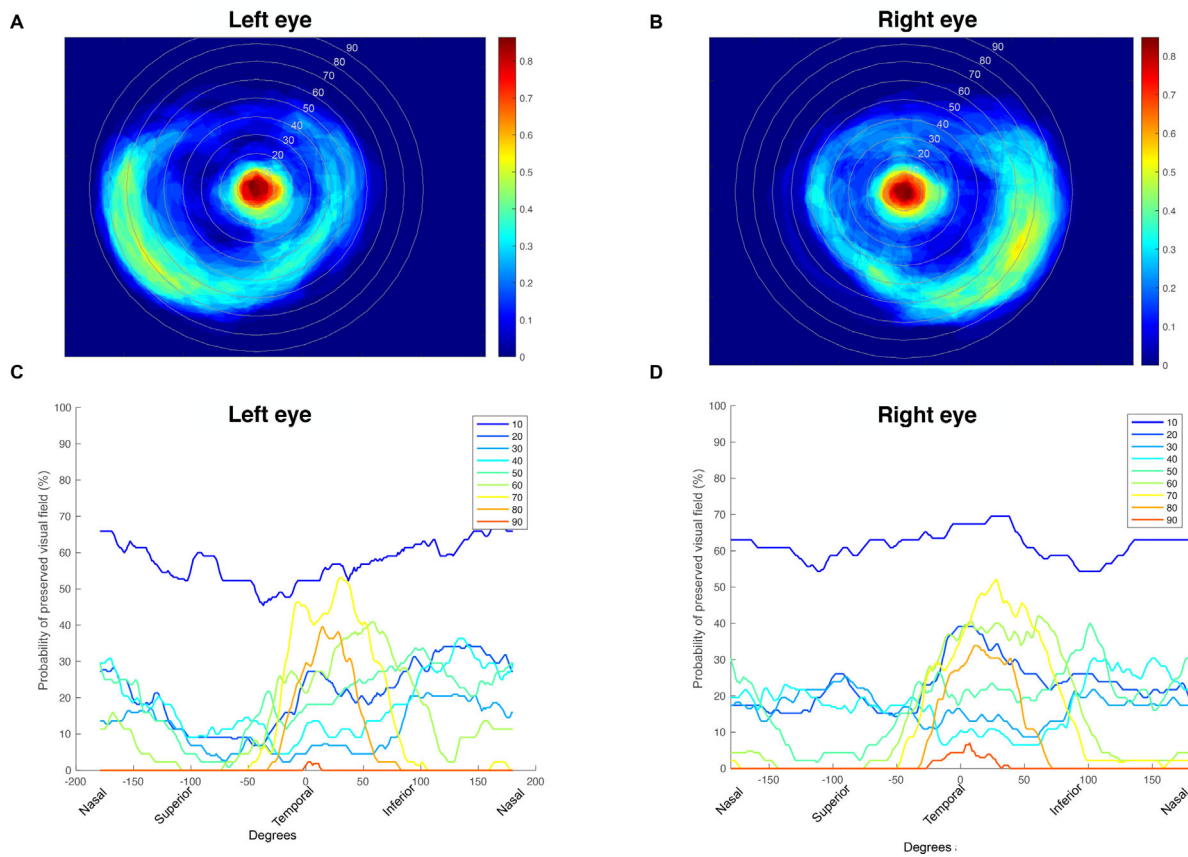
FIGURE 3. Probability maps of pVF in the subset of subjects with retained peripheral islands. Probability maps for the left (**A**) and right (**B**) eyes were generated by combining the cases with peripheral islands only and with central and peripheral islands with complete or incomplete midperipheral scotoma (circles denote the isoeccentric meridians in 10° increments). Analysis of the probability maps along the isoeccentric meridians in the left (**C**) and right (**D**) eyes revealed that the greatest probability of retained pVF was in the inferotemporal area, between 50° and 80° eccentricity from fixation.
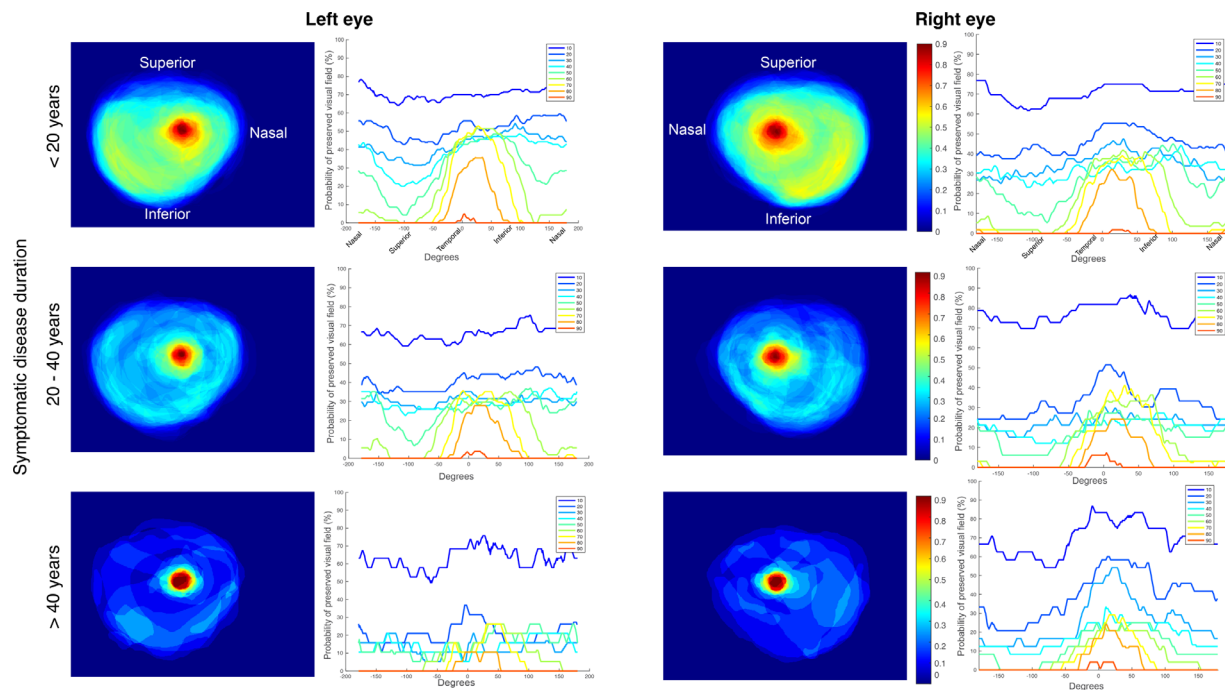

FIGURE 4. Probability maps of pVF categorized by SDD. Spatial probability maps of the left and right eyes were generated, categorized by SDD. (*Top to bottom rows*) Probability maps of subjects with SDD < 20 years, 20 to 40 years (inclusive), and >40 years. The probabilistic pattern of pVF preservation appeared to show lateral interocular symmetry and showed high probability of preservation in the peripheral inferotemporal quadrant of the VF.
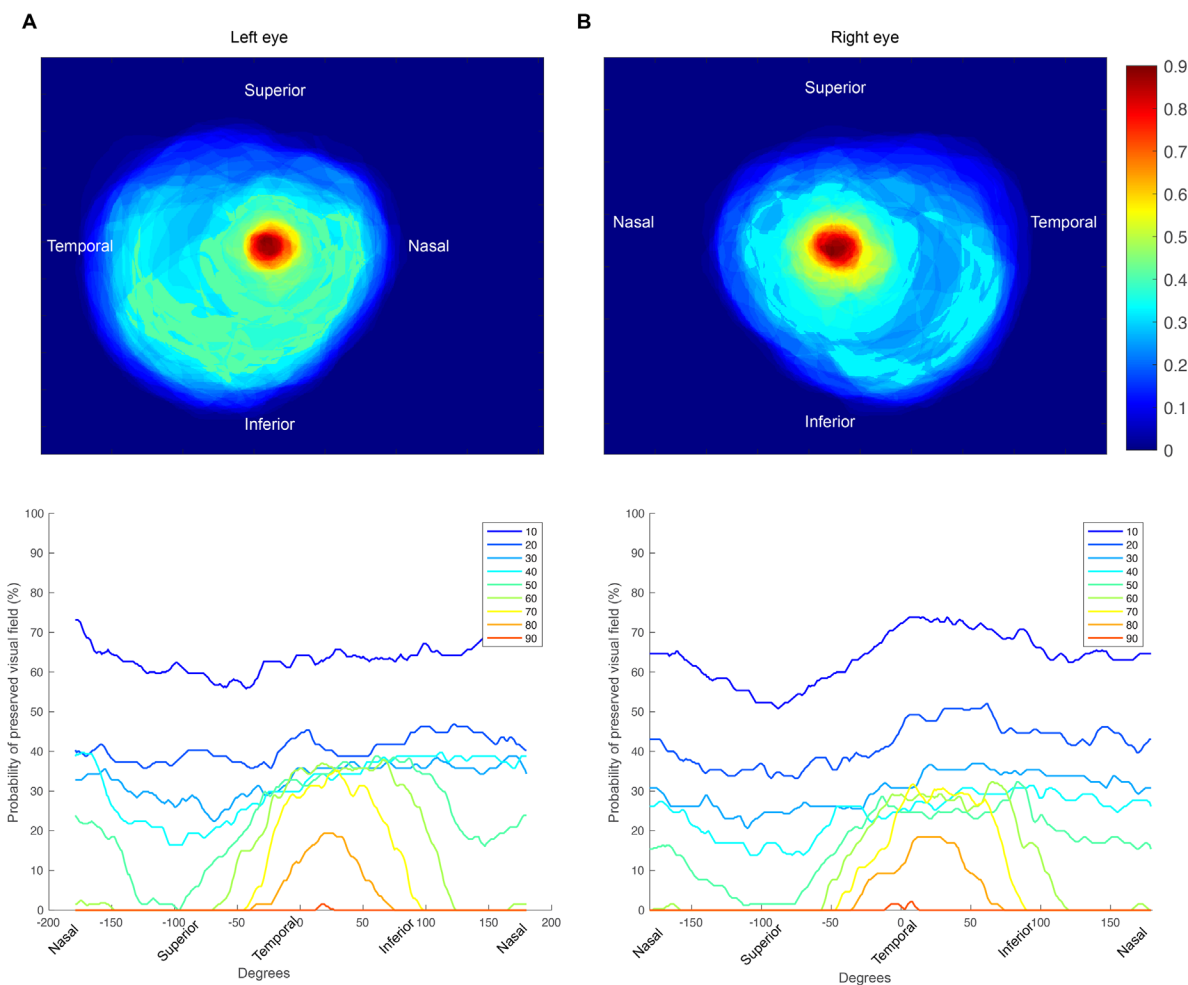
FIGURE 5. Probabilistic VF change maps generated using the longitudinal dataset. (**A**) VF change was determined by comparing baseline and follow-up GVFs in the longitudinal dataset. For each subject, a pair of baseline and follow-up V4e segmentations was compared to identify loci (pixels) where the VF was present in both maps. (**B**) The probabilistic map of VF change for the left and right eyes of all cases in the longitudinal dataset suggested that loci in the inferotemporal pVF were likely to be retained over time.
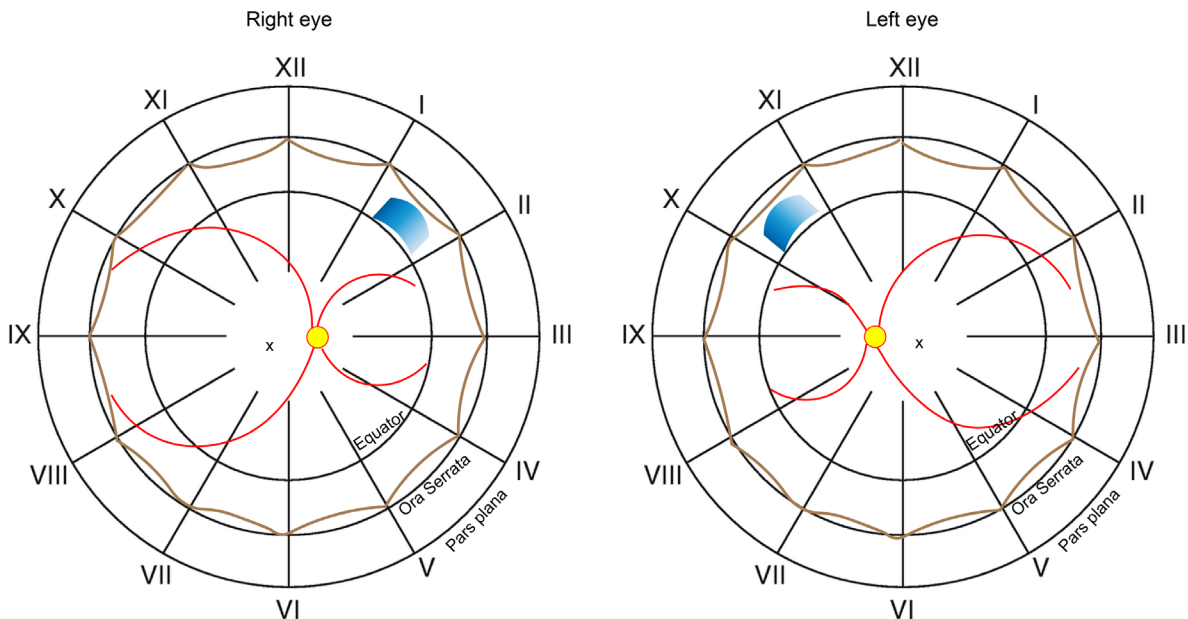

FIGURE 6. Schematic representation of the anatomical spatial correlate of resilient pVF loci in the right and left eyes. Using Dagnelie's mathematical model to convert planimetric data to solid angles,[13] a zone of the superonasal retina between the equator and the ora serrata (indicated in *blue*) was suggested as being the anatomical correlate of the pVF loci that showed maximal probability of preservation in this study.

autosomal-dominant versus others (autosomal-recessive or X-linked). Probability maps generated from these two groups showed a similar pattern of inferotemporal pVF preservation (data not shown).

Subjects were then categorized into three groups based on SDD: SDD < 20 years ($n = 72$, 47.4%), 20 to 40 years ($n = 60$, 39.5%), and >40 years ($n = 20$, 13.2%). Probability maps were generated based on the three SDD categories. All three categories demonstrated a similar spatial pattern of inferotemporal pVF preservation (Fig. 4).

A total of 65 subjects (42.8%) had repeat GVF tests at least 2 years apart from their baseline GVF (range, 3.2–5.7 years) and therefore were included in the longitudinal dataset. The mean interval between the baseline and repeat GVF was 4.8 ± 2.3 years. Comparison of the baseline and follow-up GVF identified a zone in the inferotemporal periphery of the GVF located between the 40° and 80° isoeccentric meridians and between the 20° and 50° radial axes that showed the highest probability of longitudinally retained pVF. A laterally symmetrical zone was identified in the left eye (Fig. 5).

We sought to understand the anatomical correlate of the zone of pVF retention. We leveraged the published mathematical model of Dagnelie and colleagues[13] for conversion of planimetric visual field data into solid angles and retinal areas. According to their approach, the anatomical equator of the retina corresponded to approximately 47° eccentricity from fixation. Using this method, we found that the region of retained pVF identified in the cross-sectional dataset corresponded approximately to a 1-clock-hour-wide zone of superonasal peripheral retina, located anterior to the equator (Fig. 6). This pattern was consistent across all SDD categories and in the longitudinal dataset.

Discussion

The data suggest that, when considered as a group, patients with RP tend to retain visual function in the inferotemporal pVF. Applying a mathematical model to convert pVF areas to anatomical retinal areas,[13] we found that this part of the pVF corresponded to a zone of retina in the superonasal periphery that is anterior to the equator. Although recognizing the limitations of this study, we believe that this observation provides novel information regarding the visual–spatial and anatomical localization of a zone of especially resilient peripheral retina in RP patients. The spatial pattern of pVF resilience was validated in our cross-sectional and longitudinal datasets and also when categorized by RP-related symptom duration. Our cohort is notable for its relatively large size and the inclusion of subjects with confirmed disease-causing mutation(s).

It has been speculated that light toxicity in RP patients may play a role in accelerating photoreceptor degeneration in the inferior retina, partly explaining the preferential loss of superior VF.[14–18] Other possible explanations may be related to regional functional differences among some patients with RP, as evidenced by higher dark-adaptation thresholds in the inferior than the superior retina.[19]

Another possible explanation for localized functional resilience may be related to photoreceptor density distribution. In a seminal study, Curcio et al.[20] quantified the spatial density of cone and rod photoreceptors in healthy human retinas. Cone density was highest at the foveal center and fell steeply with increasing eccentricity. However, at isoeccentric locations, the cone density was 40% to 45% higher in the nasal than in the temporal retina and increased further in the far nasal retina. In comparison, rod density was highest in the nasal and superior retina. Interpreting our findings in the context of those data, it is conceivable that the relatively high density of rod and/or cone photoreceptors in the superonasal retina may play a role in promoting localized functional resistance in the inferotemporal pVF. Interestingly, Nakagawa et al.[14] found a pattern of anatomical peripapillary nasal sparing in widefield fundus autofluorescence of RP patients ($n = 113$) and visual sensitivity preservation in an area just temporal to the physiological blind spot, thus implicating a posterior region of the nasal retina as being functionally and structurally resilient.

The information presented here may enable further research on the cellular and molecular mechanisms of localized functional resilience in this zone of retina. For example, histological, molecular, and biochemical analyses of postmortem human retinas could be focused on far superonasal retinal specimens. Insights from such studies may inform the development of genetic, cellular, and pharmacologic treatment modalities to modify RP progression. The data in our study may also inform the development of static or kinetic perimetry protocols in clinical trials, focusing on the inferotemporal pVF in greater detail than other parts of the pVF.

Calculation of areas from manual Goldmann perimetry has been addressed[13,21,22] with various software packages that can analyze scanned GVF images, such as Adobe Photoshop,[23] Engauge Digitizer,[24] Image J,[25] and FieldDigitizer.[13] These tools have been used to study the natural history of VF loss progression[26] and its progression in clinical trials targeted to retarding VF loss.[27] In this work, we developed a novel computational platform, including affine transformation and image segmentation, that enabled the aggregation of historical GVF data across cross-sectional and longitudinal cohorts. In general, prior work has emphasized qualitative descriptions of the patterns of VF loss using topography and imaging.[5,11,18] The quantitative method that we developed may facilitate future research to better understand the influence of patient-, disease-, and environment-related factors on peripheral retinal function in RP. Further analysis of this dataset by detailed genotype characteristics was beyond the scope of the current work but may be useful to generate hypotheses regarding genetic determinants of the differences in pVF preservation.

The main limitations of this study are its retrospective design, cross-sectional sample, the lack of prospective GVF testing, and the lack of masked grading by a reading center. The inclusion of genetically and phenotypically diverse RP subjects, although having the advantage of increasing cohort size, may have obscured subgroup-specific findings. The distribution of SDD in this study represents the characteristics of the cohort at our practice and may not be fully generalizable to other cohorts or populations.

A major limitation of our study pertains to the variability in GVF testing, mapping, and segmentation. Kinetic perimetry is acknowledged as showing inherent inter-visit and inter-examiner variability. Two key studies systematically investigated the variability in measurements derived from GVF testing in patients with RP. Ross et al.[28] studied GVF variability in 26 patients with RP. They found that the mean percent inter-examiner variability of perimetric area was 10% to 14%, and the mean percent inter-visit variability for the same examiner was 11% to 13%. Linear visual field measurements showed 7% to 9% mean percent variability, and the upper 95% confidence limit for linear variability

corresponded to approximately 15° radial variability. More recently, Bittner et al.[29] examined within-visit GVF variability in 37 subjects with RP by digitizing planimetric GVFs and converting them to retinal areas to correct for cartographic distortions. There was no significant change in the measured retinal areas between the first and second GVFs. The 95% coefficient of repeatability was 19.2% for the V4e isopter. The authors proposed that GVF was the method of choice for pVF measurement, provided that experienced operators conducted the testing. Incorporating information from those studies, we estimate that the 95% confidence interval around our findings of probabilistically retained pVF between the 50° and 80° isoeccentric meridians and the 30° and 50° radial axes was approximately 10° in each direction, assuming 20% retinal area variability. These values may underestimate actual variability in the current study, due to its retrospective design, in contrast to the prospective design of the reference studies.[28,29]

In summary, semiautomated computational quantitation of the spatial characteristics of pVF may be a useful platform to analyze the pVF in RP. Our data conform to prior observations that certain portions of the pVF may be relatively resistant to functional decline during RP progression and yield new information regarding the anatomical location of apparently resilient retina. Further research may reveal genetic or acquired factors that influence the rate of localized pVF loss. Understanding the cellular and molecular basis of pVF resilience may inform further research on the development of therapy to retard the rate of retinal functional decline in RP.

Acknowledgments

Disclosure: **T.P. Patel**, None; **H. Vongsachang**, None; **A. Schilling**, None; **X. Kong**, None; **M.S. Singh**, None

References

1. Hamel C. Retinitis pigmentosa. *Orphanet J Rare Dis*. 2006;1(1):40.

2. Grover S, Fishman GA, Anderson RJ, Alexander KR. Progression of visual field loss in retinitis pigmentosa. *Invest Ophthalmol Vis Sci*. 1996;37(3):S501.

3. Grover S, Fishman GA, Anderson RJ, Alexander KR, Derlacki DJ. Rate of visual field loss in retinitis pigmentosa. *Ophthalmology*. 1997;104(3):460–465.

4. Varsamidis M, Luu C, Dimitrov P, Guymer R, Ayton L. The relevance of residual visual field islands in retinitis pigmentosa. *Invest Ophthalmol Vis Sci*. 2013;54(15):668–668.

5. Grover S, Fishman GA, Brown J, Jr. Patterns of visual field progression in patients with retinitis pigmentosa. *Ophthalmology*. 1998;105(6):1069–1075.

6. Birch DG, Anderson JL. Rod visual fields in cone-rod degeneration. Comparisons to retinitis pigmentosa. *Invest Ophthalmol Vis Sci*. 1990;31(11):2288–2299.

7. Sandberg MA, Weigel-DiFranco C, Rosner B, Berson EL. The relationship between visual field size and electroretinogram amplitude in retinitis pigmentosa. *Invest Ophthalmol Vis Sci*. 1996;37(8):1693–1698.

8. Jacobson SG, Voigt WJ, Parel JM, et al. Automated light- and dark-adapted perimetry for evaluating retinitis pigmentosa. *Ophthalmology*. 1986;93(12):1604–1611.

9. Berson EL, Sandberg MA, Rosner B, Birch DG, Hanson AH. Natural course of retinitis pigmentosa over a three-year interval. *Am J Ophthalmol*. 1985;99(3):240–251.

10. Fishman GA, Bozbeyoglu S, Massof RW, Kimberling W. Natural course of visual field loss in patients with type 2 Usher syndrome. *Retina*. 2007;27(5):601–608.

11. Talib M, Dagnelie G, Boon CJF. Recording and analysis of Goldmann kinetic visual fields. *Methods Mol Biol*. 2018;1715:327–338.

12. Richards S, Aziz N, Bale S, et al. Standards and guidelines for the interpretation of sequence variants: a joint consensus recommendation of the American College of Medical Genetics and Genomics and the Association for Molecular Pathology. *Genet Med*. 2015;17(5):405–424.

13. Dagnelie G. Technical note. Conversion of planimetric visual field data into solid angles and retinal areas. *Clin Vis Sci*. 1990;5(1):95–100.

14. Nakagawa S, Oishi A, Ogino K, et al. Asymmetric cone distribution and its clinical appearance in retinitis pigmentosa. *Retina*. 2016;36(7):1340–1344.

15. Alexander KR, Fishman GA. Prolonged rod dark adaptation in retinitis pigmentosa. *Br J Ophthalmol*. 1984;68(8):561–569.

16. Cideciyan AV, Hood DC, Huang Y, et al. Disease sequence from mutant rhodopsin allele to rod and cone photoreceptor degeneration in man. *Proc Natl Acad Sci USA*. 1998;95(12):7103–7108.

17. Sakami S, Maeda T, Bereta G, et al. Probing mechanisms of photoreceptor degeneration in a new mouse model of the common form of autosomal dominant retinitis pigmentosa due to P23H opsin mutations. *J Biol Chem*. 2011;286(12):10551–10567.

18. Stone EM, Kimura AE, Nichols BE, Khadivi P, Fishman GA, Sheffield VC. Regional distribution of retinal degeneration in patients with the proline to histidine mutation in codon 23 of the rhodopsin gene. *Ophthalmology*. 1991;98(12):1806–1813.

19. Krill AE, Smith VC, Blough R, Pass A. An absolute threshold defect in the inferior retina. *Invest Ophthalmol*. 1968;7(6):701–707.

20. Curcio CA, Sloan KR, Kalina RE, Hendrickson AE. Human photoreceptor topography. *J Comp Neurol*. 1990;292(4):497–523.

21. Weleber RG, Tobler WR. Computerized quantitative analysis of kinetic visual fields. *Am J Ophthalmol*. 1986;101(4):461–468.

22. Odaka T, Fujisawa K, Akazawa K, et al. A visual field quantification system for the Goldmann Perimeter. *J Med Syst*. 1992;16(4):161–169.

23. Zahid S, Peeler C, Khan N, et al. Digital quantification of Goldmann visual fields (GVFs) as a means for genotype-phenotype comparisons and detection of progression in retinal degenerations. *Adv Exp Med Biol*. 2014;801:131–137.

24. Patel DE, Cumberland PM, Walters BC, Cortina-Borja M, Rahi JS, OPTIC Study Group. Study of Optimal Perimetric Testing in Children (OPTIC): evaluation of kinetic approaches in childhood neuro-ophthalmic disease. *Br J Ophthalmol*. 2019;103(8):1085–1091.

25. Maamari RN, D'Ambrosio MV, Joseph JM, Tao JP. The efficacy of a novel mobile phone application for Goldmann ptosis visual field interpretation. *Ophthalmic Plast Reconstr Surg*. 2014;30(2):141–145.

26. Massof R, Dagnelie G, Benzschawel T, Palmer R, Stein D. First order dynamics of visual field loss in retinitis pigmentosa. *Clin Vis Sci*. 1990;5:1–26.

27. Berson EL, Rosner B, Sandberg MA, et al. A randomized trial of vitamin A and vitamin E supplementation for retinitis pigmentosa. *Arch Ophthalmol*. 1993;111(6):761–772.
28. Ross DF, Fishman GA, Gilbert LD, Anderson RJ. Variability of visual field measurements in normal subjects and patients with retinitis pigmentosa. *Arch Ophthalmol*. 1984;102(7):1004–1010.
29. Bittner AK, Iftikhar MH, Dagnelie G. Test-retest, within-visit variability of Goldmann visual fields in retinitis pigmentosa. *Invest Ophthalmol Vis Sci*. 2011;52(11):8042–8046.